Available online at www.sciencedirect.com
SCIENCE DIRECT®
Comput. Methods Appl. Mech. Engrg. 195 (2006) 1050–1074
Computer methods in applied mechanics and engineering
www.elsevier.com/locate/cma

Response variability of stochastic frame structures using evolutionary field theory

Vissarion Papadopoulos [a,*], George Deodatis [b]

[a] Institute of Structural Analysis and Seismic Research, National Technical University of Athens, 9 Iroon Polytechneiou, Zografou Campus, Athens 15780, Greece
[b] Department of Civil Engineering and Engineering Mechanics, Columbia University, New York, NY 10027, USA

Received 8 November 2004; received in revised form 31 March 2005; accepted 8 April 2005

Abstract

The integral form for the variance of the response of stochastic statically indeterminate structural systems involving the so-called variability response function (VRF) and the spectral density function of the stochastic field modelling the uncertain system properties is established for the first time in this paper using evolutionary spectra theory. The VRF is a function depending on deterministic parameters related to the geometry, boundary conditions, (mean) material properties and loading of the structural system. No approximations are involved in the derivation of the integral form. However, a conjecture has to be made that is validated using Monte Carlo simulations. The uncertain system property considered is the inverse of the elastic modulus (flexibility). Closed-form expressions can be derived in principle for the VRF of any statically determinate or indeterminate frame system using a flexibility-based formulation. Alternatively, a fast Monte Carlo simulation approach is provided to numerically evaluate the VRF. It is shown in closed-form and numerically that the VRF for statically indeterminate structures is a function of the standard deviation σ_{ff} of the stochastic field modeling the inverse of the elastic modulus. Although the VRF depends on σ_{ff}, it appears to be independent of the functional form of the spectral density function of the stochastic field modeling the uncertain system properties. For statically determinate structures, the VRF is independent of σ_{ff}. The integral form can be used to compute the variance of the system response as well as its upper bound with minimal computational effort. It also provides an excellent insight into the mechanisms controlling the response variability. The upper bounds for the response variance are spectral- and probability-distribution-free requiring knowledge of only the variance of the inverse of the elastic modulus. The proposed bounds are realizable in the sense that it is possible to determine the probabilistic characteristics of the stochastic field that produces them. Several numerical examples are provided demonstrating the capabilities of the methodology.

* Corresponding author.
E-mail addresses: vpapado@central.ntua.gr (V. Papadopoulos), deodatis@civil.columbia.edu (G. Deodatis).

0045-7825/$ - see front matter © 2005 Elsevier B.V. All rights reserved.
doi:10.1016/j.cma.2005.04.003

Keywords: Variability response function; Stochastic finite element analysis; Non-homogeneous stochastic fields; Upper bounds; Monte Carlo simulation

1. Introduction

The analysis of stochastic systems with material/geometric properties modelled by random fields has been the subject of extensive research in the past two decades. The majority of the work has focused on developing stochastic finite element methodologies (SFEM) for the numerical solution of the stochastic differential equations involved in the problem. By far, the most widely used SFEM approaches are approximate expansion/perturbation based methods. Although such methods have proven to be highly accurate and computationally efficient for a variety of problems, there is still a wide range of problems in stochastic mechanics involving combinations of strong non-linearities, large variations of system properties and non-Gaussian system properties that can be solved with reasonable accuracy only through a computationally expensive Monte Carlo simulation approach.

Whether an expansion/perturbation based approach or a Monte Carlo simulation methodology is used to estimate the response variability of a stochastic system, it is necessary to know the probability distribution function (PDF) and the spectral/correlation characteristics of the stochastic system properties. In most practical engineering applications, there is a lack of experimental data that would enable a quantification of such probabilistic characteristics of the stochastic system properties. Taking into account that many researchers have clearly demonstrated that both the correlation structure and the PDF of the material/geometric properties can have a significant (and in certain cases dramatic) effect on the stochastic response, a SFEM or Monte Carlo analysis will not provide particularly useful results for real-life applications when the probabilistic characteristics of the system properties are arbitrarily assumed.

A common approach to address the aforementioned problem is to perform a sensitivity analysis with respect to the various parameters controlling the probabilistic characteristics of the stochastic system properties. Although such an approach has obvious advantages, it also has certain drawbacks. First, the computational effort increases drastically as the number and range of the various parameters examined expand. Then, there is no real insight on the effect of the various parameters on the response variability of the system. And finally, it is practically impossible to determine upper bounds on the response variability as the number of combinations of the various parameters is essentially infinite.

To address all three of the above drawbacks, the concept of variability response function (VRF) was introduced in the late 1980s. The basic idea associated with the VRF is to express the variance of the response (i.e. displacement) in the following integral form:

$$\mathrm{Var}[u] = \int_{-\infty}^{\infty} \mathrm{VRF}(\kappa) S_{ff}(\kappa)\, \mathrm{d}\kappa, \tag{0a}$$

where the VRF is a function depending on deterministic parameters related to the geometry, boundary conditions, (mean) material properties and loading of the structural system, $S_{ff}(\kappa)$ is the spectral density function of the stochastic field modeling the uncertain material/geometric properties, and κ is the wave number.

It is straightforward to see how the concept of the VRF in conjunction with the integral form in Eq. (0a) addresses all three drawbacks mentioned above. Once the VRF is determined, the variance of the response can be estimated very easily through a simple integration given any form of the spectral density function $S_{ff}(\kappa)$ (the VRF is usually a smooth function of κ). Eq. (0a) also provides an excellent insight of the effect of the form of the spectral density function of the stochastic field modeling the uncertain material/geometric properties on the response variability. Finally, a spectral- and probability-distribution-free upper bound for the response variance can be computed in a straightforward way as:

$$\mathrm{Var}[u] \leqslant \mathrm{VRF}(\kappa^{\max})\sigma_{ff}^2 \tag{0b}$$

with $\kappa^{\max}$ being the wave number where the VRF attains its maximum value and σ_{ff}^2 being the variance of the stochastic field modeling the material/geometric properties.

Early work determined the VRF for a wide range of problems (beams, frames, plane stress/strain, plate bending, random eigenvalue problem) using some kind of first-order approximation (usually of the response displacement). An immediate consequence was that even the existence of the integral form in Eq. (0a) depended on this approximation. The uncertain system property in this early work was always the elastic modulus. A more detailed description of the early developments in this field, including a list of relevant references until the present, can be found in [3] where it was attempted for the first time to establish the integral form in Eq. (0a) without having to go through a first-order approximation. The key was to consider the inverse of the elastic modulus as the uncertain system property. For the case of statically determinate beam structures, the existence of the integral form in Eq. (0a) was easily established in a rigorous mathematical way and closed-form expressions were provided for the VRF. For statically indeterminate beam structures, however, a conjecture had to be made about the existence of an integral form like the one in Eq. (0a) and the VRF was subsequently estimated numerically. The validity of this conjecture was demonstrated numerically through a brute-force optimization scheme involving the computation of upper bounds of the response variance. Consequently, because the conjecture was based mostly on insight and because of the process followed to validate it, Papadopoulos et al. [3] used Eq. (0a) in an ad hoc way to determine only upper bounds of the response variance (and not the response variance itself).

The present paper complements and extends the work done in [3] in the following ways. First, the integral form in Eq. (0a) for statically indeterminate structures is formulated in a different way using the concept of non-homogeneous evolutionary fields developed by Priestley [4]. Although a rigorous mathematical proof of the existence of the integral form in Eq. (0a) is still elusive for statically indeterminate structures, a different conjecture is made now regarding the existence of a non-homogeneous evolutionary stochastic field involving the uncertain elastic properties. Furthermore, this alternative conjecture is now validated numerically by computing the response variance through Eq. (0a) and comparing it with Monte Carlo simulation predictions. There is still no first-order approximation involved as the inverse of the elastic modulus is again considered as the uncertain system property. Closed-form expressions can be established in principle for the variability response function of any statically determinate or indeterminate frame system using a flexibility-based formulation. In contrast to the conclusions in [3], it is shown here that the VRF for statically indeterminate structures is a function of the standard deviation σ_{ff} of the stochastic field modeling the inverse of the elastic modulus. The dependence of VRF on σ_{ff} is negligible in some cases and this is the reason that it was not detected numerically in [3]. In the present paper, the dependence of the VRF on σ_{ff} for statically indeterminate structures is established in closed-form expressions. It is pointed out that although the VRF depends on σ_{ff}, it appears to be independent of the functional form of the spectral density function $S_{ff}(\kappa)$. For statically determinate structures, the VRF is independent of σ_{ff} as well.

The integral form in Eq. (0a) is therefore established in this paper using a different formulation involving an alternative conjecture compared to [3]. In addition, the validation of the conjecture is done in a much stricter way in this paper: by comparing the response variance predictions of Eq. (0a) with Monte Carlo simulations (compared to a brute-force optimization validation in [3] involving the upper bound of the response variance). Consequently, Eq. (0a) is used in this paper with confidence to compute the variance of the response through a simple integration, as well as to estimate its upper bound (compare to [3] where it was used only to estimate upper bounds).

The upper bounds established in this study for the response variability are spectral- and probability-distribution-free requiring knowledge of only the variance of the inverse of the elastic modulus. It should be mentioned that the variance of the inverse of the elastic modulus can be obtained as easily as the variance of the elastic modulus using the same experimental data. The proposed bounds are realizable in the sense that

it is possible to determine the probabilistic characteristics (spectral density function and marginal probability distribution function) of the stochastic field (modeling the inverse of the elastic modulus) that produces them. Furthermore, it is possible to fully determine also the corresponding stochastic field modeling the elastic modulus that produces these bounds.

Finally, it should be mentioned that the approach used in this paper to model the beam flexibility instead of its rigidity has already been followed in a small number of earlier studies (e.g. [1]). In these studies, exact expressions for the response variance were established for simple statically determinate beams under static loading (but not in the form of Eq. (0a) involving the variability response function).

2. Statically determinate beams

Consider the statically determinate beam of length L shown in Fig. 1, carrying a deterministic uniformly distributed load Q_0. The inverse of the elastic modulus of the beam is assumed to vary randomly along its length according to the following expression:

$$\frac{1}{E(x)} = F_0(1 + f(x)), \tag{1}$$

where E is the elastic modulus, F_0 is the mean value of the inverse of E, and $f(x)$ is a zero-mean homogeneous stochastic field modeling the variation of $1/E$ around its mean value F_0.

The response displacement of the beam $u(x)$ is given by:

$$u(x) = \frac{F_0 Q_0}{2I}\int_0^x (x-\xi)(L-\xi)^2(1+f(\xi))\,\mathrm{d}\xi = \int_0^x g(x,\xi)(1+f(\xi))\,\mathrm{d}\xi, \tag{2}$$

where I is the moment of inertia and:

$$g(x,\xi) = \frac{F_0 Q_0}{2I}(x-\xi)(L-\xi)^2. \tag{3}$$

As described in detail in [3], the variance of the response displacement can be expressed in the following form:

$$\mathrm{Var}[u(x)] = \int_{-\infty}^{\infty} \mathrm{VRF}(x,\kappa) S_{ff}(\kappa)\,\mathrm{d}\kappa, \tag{4}$$

where the variability response function (VRF) is given by:

$$\mathrm{VRF}(x,\kappa) = \left|\int_0^x g(x,\xi)\mathrm{e}^{\mathrm{i}\kappa\xi}\,\mathrm{d}\xi\right|^2 \tag{5}$$

and $S_{ff}(\kappa)$ denotes the power spectral density function of stochastic field $f(x)$. As shown in [3], the expressions for the $\mathrm{Var}[u(x)]$ and the VRF is Eqs. (4) and (5) are exact analytic expressions as no approximations

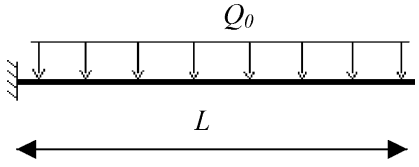

Fig. 1. Configuration of statically determinate beam.

were made for their derivation. Furthermore, similar expressions can be established for any statically determinate beam with any kind of boundary and loading conditions.

3. Statically indeterminate beams

Consider now the statically indeterminate beam of length L shown in Fig. 2, carrying a deterministic uniformly distributed load Q_0. The inverse of the elastic modulus is again assumed to vary randomly along the length of the beam according to Eq. (1).

Using a force (flexibility) method formulation as in [3], the response displacement of this beam $u(x)$ can be expressed as:

$$u(x) = u_0(x) - Ru_1(x), \tag{6}$$

where $u_0(x)$ is the deflection of the associated statically determinate beam with uniform load Q_0 obtained by removing the simple support at the right end of the beam in Fig. 2, $u_1(x)$ is the deflection of the same associated statically determinate beam due to a unit concentrated force acting at $x = L$, and R is the redundant force (vertical reaction at the right end of the beam in Fig. 2).

Eq. (6) is then written as follows:

$$\begin{aligned} u(x) &= \frac{F_0 Q_0}{2I}\int_0^x (x-\xi)(L-\xi)^2(1+f(\xi))\,\mathrm{d}\xi - \frac{F_0 R}{I}\int_0^x (x-\xi)(L-\xi)(1+f(\xi))\,\mathrm{d}\xi \\ &= \int_0^x g_0(x,\xi)(1+f(\xi))\,\mathrm{d}\xi + \int_0^x g_1(x,\xi)R(1+f(\xi))\,\mathrm{d}\xi, \end{aligned} \tag{7a}$$

where

$$g_0(x,\xi) = \frac{F_0 Q_0}{2I}(x-\xi)(L-\xi)^2 \quad \text{and} \quad g_1(x,\xi) = -\frac{F_0}{I}(x-\xi)(L-\xi). \tag{7b}$$

The redundant force R is a random variable that can be computed from the boundary condition at $x = L$ as:

$$u(x=L) = 0 \Rightarrow u_0(x=L) = Ru_1(x=L) \Rightarrow R = \frac{\dfrac{Q_0}{2}\displaystyle\int_0^L (L-\xi)^3(1+f(\xi))\,\mathrm{d}\xi}{\displaystyle\int_0^L (L-\xi)^2(1+f(\xi))\,\mathrm{d}\xi}. \tag{8}$$

Taking now the expectation on both sides of Eq. (7a), the mean value of $u(x)$ is computed as follows:

$$\varepsilon[u(x)] = \int_0^x g_0(x,\xi)\,\mathrm{d}\xi + \int_0^x g_1(x,\xi)\varepsilon[R(1+f(\xi))]\,\mathrm{d}\xi. \tag{9}$$

Combining now Eqs. (7a) and (9), the following expression is written for $u(x) - \varepsilon[u(x)]$:

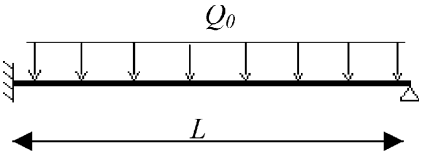

Fig. 2. Configuration of fixed-simply supported statically indeterminate beam.

$$u(x) - \varepsilon[u(x)] = \int_0^x \{g_0(x,\xi)(1+f(\xi)) + g_1(x,\xi)R(1+f(\xi)) - g_0(x,\xi) - g_1(x,\xi)\varepsilon[R(1+f(\xi))]\}\,\mathrm{d}\xi$$
$$= \int_0^x \{g_0(x,\xi)f(\xi) + g_1(x,\xi)p(\xi)\}\,\mathrm{d}\xi, \tag{10}$$

where

$$p(x) = R(1+f(x)) - \varepsilon[R(1+f(x))] \tag{11}$$

can be easily shown to be a zero-mean, non-homogeneous stochastic field. The variance of the response displacement $u(x)$ is then computed as:

$$\mathrm{Var}[u(x)] = \varepsilon\{(u(x) - \varepsilon[u(x)])^2\}$$
$$= \int_0^x \int_0^x \{g_0(x,\xi_1)g_0(x,\xi_2)R_{ff}(\xi_1-\xi_2) + g_1(x,\xi_1)g_1(x,\xi_2)R_{pp}(\xi_1,\xi_2)$$
$$+ g_0(x,\xi_1)g_1(x,\xi_2)\varepsilon[f(\xi_1)p(\xi_2)] + g_0(x,\xi_2)g_1(x,\xi_1)\varepsilon[p(\xi_1)f(\xi_2)]\}\,\mathrm{d}\xi_1\,\mathrm{d}\xi_2, \tag{12}$$

where $R_{ff}(\xi_1-\xi_2)$ and $R_{pp}(\xi_1,\xi_2)$ denote the autocorrelation functions of stochastic fields $f(x)$ and $p(x)$ respectively. The quantities $\varepsilon[f(\xi_1)p(\xi_2)]$ and $\varepsilon[p(\xi_1)f(\xi_2)]$ in Eq. (12) are the cross-correlation functions $R_{fp}(\xi_1,\xi_2)$ and $R_{pf}(\xi_1,\xi_2)$ of stochastic fields $f(x)$ and $p(x)$. Since by definition $R_{pf}(\xi_1,\xi_2) = R_{fp}(\xi_2,\xi_1)$, Eq. (12) can be rewritten as follows:

$$\mathrm{Var}[u(x)] = \int_0^x \int_0^x \{g_0(x,\xi_1)g_0(x,\xi_2)R_{ff}(\xi_1-\xi_2) + g_1(x,\xi_1)g_1(x,\xi_2)R_{pp}(\xi_1,\xi_2)$$
$$+ 2g_0(x,\xi_1)g_1(x,\xi_2)R_{fp}(\xi_1,\xi_2)\}\,\mathrm{d}\xi_1\,\mathrm{d}\xi_2. \tag{13}$$

The challenge at this point is to express $\mathrm{Var}[u(x)]$ of the statically indeterminate beam in a form similar to the one derived in Eqs. (4) and (5) for the statically determinate beam.

3.1. Description of the non-homogeneous stochastic field $p(x)$

It will be shown that stochastic field $p(x)$ defined in Eq. (11) can be expressed as a non-homogeneous stochastic field with evolutionary power [4] that depends on the geometry, the loading and boundary conditions of the beam (all assumed to be deterministic), as well as on the spectral density function $S_{ff}(\kappa)$ of stochastic field $f(x)$ (assumed to be homogeneous).

Assuming that stochastic field $p(x)$ is oscillatory [4], it can be expressed in the following form:

$$p(x) = \int_{-\infty}^{\infty} A(x,\kappa)\mathrm{e}^{\mathrm{i}\kappa x}\,\mathrm{d}Z(\kappa), \tag{14a}$$

where $A(x,\kappa)$ is a modulating function and $Z(\kappa)$ an orthogonal field with:

$$\varepsilon[(\mathrm{d}Z(\kappa))^2] = \mathrm{d}S_{pp}(\kappa). \tag{14b}$$

The evolutionary power spectrum of $p(x)$, $S^{\mathrm{E}}_{pp}(x,\kappa)$, is then given by:

$$S^{\mathrm{E}}_{pp}(x,\kappa) = A^2(x,\kappa)S_{pp}(\kappa), \tag{15}$$

where $S_{pp}(\kappa)$ is a standard (homogeneous) power spectral density function.

The evolutionary power spectrum of $p(x)$ in the above equation can be expressed alternatively as:

$$S^{\mathrm{E}}_{pp}(x,\kappa) = [A(x,\kappa)]^2 S_{pp}(\kappa) = [A^*(x,\kappa)]^2 S_{ff}(\kappa). \tag{16}$$

Eq. (16) displays two alternative evolutionary power spectral representations of the non-homogeneous field $p(x)$. If the modulating function and standard (homogeneous) power spectral density function of one of these representations is known, then, assuming the power spectral density function of the other is given, its modulating function can be easily determined using Eq. (16). From the (infinite) alternative evolutionary power spectral representations of $p(x)$, the one involving $S_{ff}(\kappa)$ (shown in Eq. (16)) is selected for the following reason: inspection of Eq. (11) indicates that stochastic fields $f(x)$ and $p(x)$ have similar frequency contents.

Following [4], the autocorrelation function of the non-homogeneous field $p(x)$ is expressed as follows:

$$R_{pp}(x_1,x_2)=\int_{-\infty}^{\infty}A^*(x_1,\kappa)A^*(x_2,\kappa)\mathrm{e}^{\mathrm{i}\kappa(x_2-x_1)}S_{ff}(\kappa)\,\mathrm{d}\kappa, \tag{17}$$

while the cross-correlation function $R_{fp}(x_1,x_2)$ between the homogeneous field $f(x)$ and the non-homogeneous field $p(x)$ is given by:

$$R_{fp}(x_1,x_2)=\int_{-\infty}^{\infty}\widetilde{A}(x_1,\kappa)A^*(x_2,\kappa)\mathrm{e}^{\mathrm{i}\kappa(x_2-x_1)}S_{fp}(\kappa)\,\mathrm{d}\kappa=\int_{-\infty}^{\infty}A^*(x_2,\kappa)\mathrm{e}^{\mathrm{i}\kappa(x_2-x_1)}S_{fp}(\kappa)\,\mathrm{d}\kappa, \tag{18}$$

where $S_{fp}(\kappa)$ is a standard (homogeneous) cross-spectral density function and $\widetilde{A}(x,\kappa)$ denotes the modulating function of the homogeneous field $f(x)$ which is equal to unity ($\widetilde{A}(x,\kappa)=1$).

The evolutionary cross-spectrum between $f(x)$ and $p(x)$ is then given by:

$$S^{\mathrm{E}}_{fp}(x,\kappa)=\widetilde{A}(x,\kappa)A^*(x,\kappa)S_{fp}(\kappa)=A^*(x,\kappa)S_{fp}(\kappa). \tag{19}$$

In general, the homogeneous cross-spectral density function $S_{fp}(\kappa)$ is a complex function of κ:

$$S_{fp}(\kappa)=C_{fp}(\kappa)-\mathrm{i}Q_{fp}(\kappa), \tag{20}$$

where $C_{fp}(\kappa)$ denotes the co-spectrum (a real-valued even function of κ) and $Q_{fp}(\kappa)$ denotes the quad-spectrum (a real-valued odd function of κ).

Substituting Eq. (20) into Eq. (18), the cross-correlation function $R_{fp}(x_1,x_2)$ becomes:

$$R_{fp}(x_1,x_2)=\int_{-\infty}^{\infty}A^*(x_2,\kappa)\mathrm{e}^{\mathrm{i}\kappa(x_2-x_1)}C_{fp}(\kappa)\,\mathrm{d}\kappa-\mathrm{i}\left(\int_{-\infty}^{\infty}A^*(x_2,\kappa)\mathrm{e}^{\mathrm{i}\kappa(x_2-x_1)}Q_{fp}(\kappa)\,\mathrm{d}\kappa\right). \tag{21}$$

Using now a procedure similar to the one in Eqs. (16) and (21) can be expressed alternatively as:

$$R_{fp}(x_1,x_2)=\int_{-\infty}^{\infty}A^{**}(x_2,\kappa)\mathrm{e}^{\mathrm{i}\kappa(x_2-x_1)}S_{ff}(\kappa)\,\mathrm{d}\kappa-\mathrm{i}\left(\int_{-\infty}^{\infty}A^{***}(x_2,\kappa)\mathrm{e}^{\mathrm{i}\kappa(x_2-x_1)}S_{ff}(\kappa)\,\mathrm{d}\kappa\right), \tag{22}$$

where $A^{**}(x,\kappa)$ is an even function of κ and $A^{***}(x,\kappa)$ is an odd function of κ (note that $A^*(x,\kappa)$ is an even function of κ).

The corresponding alternative expression of the evolutionary cross-spectrum $S^{\mathrm{E}}_{fp}(x,\kappa)$ is:

$$S^{\mathrm{E}}_{fp}(x,\kappa)=A^*(x,\kappa)C_{fp}(\kappa)-\mathrm{i}A^*(x,\kappa)Q_{fp}(\kappa)=A^{**}(x,\kappa)S_{ff}(\kappa)-\mathrm{i}A^{***}(x,\kappa)S_{ff}(\kappa). \tag{23}$$

3.2. Closed-form expression for the variance of the response displacement

Substituting finally Eqs. (17) and (22) into Eq. (13), the following expression for the variance of the response displacement can be established:

$$\mathrm{Var}[u(x)]=\int_{-\infty}^{\infty}\mathrm{VRF}(x,\kappa,\sigma_{ff})S_{ff}(\kappa)\,\mathrm{d}\kappa, \tag{24}$$

where

$$\mathrm{VRF}(x,\kappa,\sigma_{ff}) = \int_0^x \int_0^x \{g_0(x,\xi_1)g_0(x,\xi_2) + g_1(x,\xi_1)g_1(x,\xi_2)A^*(\xi_1,\kappa)A^*(\xi_2,\kappa) + 2g_0(x,\xi_1)g_1(x,\xi_2)A^{**}(\xi_2,\kappa) + 2g_0(x,\xi_1)g_1(x,\xi_2)(-\mathrm{i})A^{***}(\xi_2,\kappa)\}\mathrm{e}^{\mathrm{i}\kappa(\xi_2-\xi_1)}\,\mathrm{d}\xi_1\,\mathrm{d}\xi_2 \tag{25}$$

or

$$\begin{aligned}\mathrm{VRF}(x,\kappa,\sigma_{ff}) = \int_0^x \int_0^x \{&g_0(x,\xi_1)g_0(x,\xi_2)\cos[\kappa(\xi_2-\xi_1)] \\ &+ g_1(x,\xi_1)g_1(x,\xi_2)A^*(\xi_1,\kappa)A^*(\xi_2,\kappa)\cos[\kappa(\xi_2-\xi_1)] \\ &+ 2g_0(x,\xi_1)g_1(x,\xi_2)A^{**}(\xi_2,\kappa)\cos[\kappa(\xi_2-\xi_1)] \\ &+ 2g_0(x,\xi_1)g_1(x,\xi_2)A^{***}(\xi_2,\kappa)\ \sin[\kappa(\xi_2-\xi_1)]\}\,\mathrm{d}\xi_1\,\mathrm{d}\xi_2.\end{aligned} \tag{26}$$

It is reminded that $A^*(x,\kappa)$ and $A^{**}(x,\kappa)$ are both even functions of κ and $A^{***}(x,\kappa)$ is an odd function of κ, so that $\mathrm{VRF}(x,\kappa,\sigma_{ff})$ is an overall even function of κ.

The integral form of $\mathrm{Var}[u(x)]$ in Eq. (24) and the closed-form expression of $\mathrm{VRF}(x,\kappa,\sigma_{ff})$ in Eq. (26) are based on the following two assumptions that have not been proven yet: (1) the *existence* of the evolutionary power spectral representation of stochastic field $p(x)$, and (2) the *independence* of $\mathrm{VRF}(x,\kappa,\sigma_{ff})$ from $S_{ff}(\kappa)$. Regarding the second assumption, it has to be demonstrated that the alternative evolutionary power spectral expressions in Eqs. (16) and (23) do not yield an expression for $\mathrm{VRF}(x,\kappa,\sigma_{ff})$ that depends on $S_{ff}(\kappa)$ (although the closed-form expression in Eq. (26) will be shown to depend of σ_{ff}). The aforementioned two assumptions cannot be proven in a rigorous mathematical way. Consequently, we consider that they form a conjecture that is validated in the following way.

If the assumptions of existence and independence mentioned above are valid, then it should be possible to estimate $\mathrm{VRF}(x,\kappa,\sigma_{ff})$ using the so-called fast Monte Carlo simulation (FMCS) approach (e.g. [3]) that computes the variability response function at each wave number κ by considering that stochastic field $f(x)$ modeling the inverse of the elastic modulus becomes a random sinusoid. The basic steps of this approach are described in the following.

1. Generate N sample functions of a random sinusoid with standard deviation σ_{ff} and wave number $\bar{\kappa}$ modeling the inverse of the elastic modulus:
$$f_j(x) = \sqrt{2}\sigma_{ff}\cos(\bar{\kappa}x + \phi_j); \quad j = 1,2,\ldots,N, \tag{27}$$
where ϕ_j are random phase angles uniformly distributed in the range $[0, 2\pi]$.
2. Using these N generated sample functions of $f_j(x)$ and the exact analytic deterministic expression for the response displacement of the statically indeterminate beam (Eqs. (7) and (8)), it is straightforward to compute the corresponding N displacement responses. Then, the variance of the response $\mathrm{Var}[u(x)]_{\bar{\kappa}}$ can be easily estimated numerically for a specific value of $\bar{\kappa}$ by ensemble averaging the N computed responses.
3. The value of the variability response function of the statically indeterminate beam at wave number $\bar{\kappa}$ is then computed from:
$$\mathrm{VRF}(x,\bar{\kappa},\sigma_{ff}) = \frac{\mathrm{Var}[u(x)]_{\bar{\kappa}}}{\sigma_{ff}^2}. \tag{28}$$
4. Steps 1–3 are repeated for different values of the wave number $\bar{\kappa}$ of the random sinusoid and the $\mathrm{VRF}(x,\kappa,\sigma_{ff})$ is computed over a wide range of wave numbers, wave number by wave number.

Eq. (28) is a direct consequence of Eq. (24), when the stochastic field $f(x)$ modeling the inverse of the elastic modulus becomes a random sinusoid.

Once $\mathrm{VRF}(x, \kappa, \sigma_{ff})$ is computed numerically for a given value of σ_{ff} as described above, the variance of the response displacement $\mathrm{Var}[u(x)]$ for a given spectral density function $S_{ff}(\kappa)$ of stochastic field $f(x)$ (having of course the same value of σ_{ff}) is easily determined through the simple integration depicted in Eq. (24). If either one of the two assumptions of existence and independence is not valid, the integration in Eq. (24)—using the numerically computed $\mathrm{VRF}(x, \kappa, \sigma_{ff})$ via FMCS—should lead to an erroneous value for $\mathrm{Var}[u(x)]$. As it is easy to compute the exact value of $\mathrm{Var}[u(x)]$ through brute-force Monte Carlo simulations (by simulating sample realizations of $f(x)$ according to a prescribed $S_{ff}(\kappa)$ and probability distribution function (PDF), solving the resulting beam problems deterministically, and estimating eventually the variance of the response displacement through ensemble averaging), it is also straightforward to verify whether the integration in Eq. (24) is providing the right answers for $\mathrm{Var}[u(x)]$.

The validity of the two assumptions of existence and independence will be therefore demonstrated numerically by estimating $\mathrm{Var}[u(x)]$ using the integration in Eq. (24) and through brute-force Monte Carlo simulations, and showing that the results are identical. Several different combinations of $S_{ff}(\kappa)$ and PDF will be considered for a set of different values of σ_{ff}. It is particularly interesting to note that the integral form for $\mathrm{Var}[u(x)]$ in Eq. (24) indicates that the variance of the response depends only on the spectral density function of stochastic field $f(x)$ modeling the inverse of the elastic modulus, and not on its probability distribution function.

3.2.1. Numerical demonstration of the validity of the assumptions of existence and independence

Consider the statically indeterminate beam shown in Fig. 2 having length $L = 10$ m and carrying a (deterministic) uniformly distributed load $Q_0 = 1000$ N/m. The inverse of the elastic modulus of the beam is assumed to vary randomly along its length according to Eq. (1) with $F_0 = 8 \times 10^{-9}$ m^2/N and $I = 0.1$ m^4.

Fig. 3 displays plots of $\mathrm{VRF}(x = L/2, \kappa, \sigma_{ff})$ for various values of the standard deviation σ_{ff}, calculated using the FMCS approach described earlier. These plots indicate that the VRF is a function of the standard deviation σ_{ff}. However, the differences observed among the four VRF curves obtained for the four values of σ_{ff} considered are relatively small (and become negligible for $\sigma_{ff} < 0.4$).

Three different non-Gaussian stochastic fields are selected to model $f(x)$ for the brute-force Monte Carlo simulations: (1) truncated Gaussian field, (2) lognormal translation field, and (3) triangular PDF translation field. All three of the aforementioned non-Gaussian fields are obtained from underlying Gaussian fields (denoted by $g(x)$) with the following two spectral density functions:

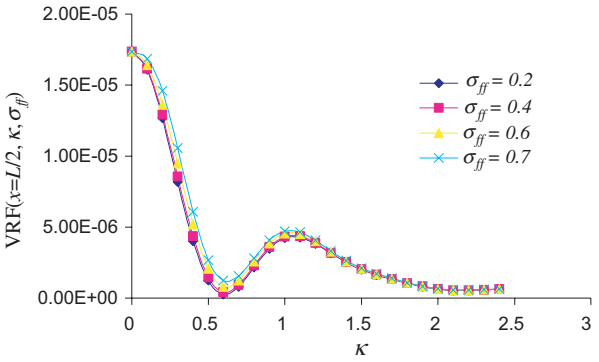

Fig. 3. Variability response function calculated using the FMCS approach for the beam shown in Fig. 2. Four different values of σ_{ff} are considered.

$$\text{SDF1:} \quad S_{gg}(\kappa) = \frac{1}{4}\sigma_{gg}^2 b^3 \kappa^2 \mathrm{e}^{-b|\kappa|}, \tag{29}$$

$$\text{SDF2:} \quad S_{gg}(\kappa) = \frac{1}{2\pi}\sigma_{gg}^2 \sqrt{\pi b}\,\mathrm{e}^{-\frac{1}{4}b\kappa^2}. \tag{30}$$

Spectrum SDF1 has zero power at $\kappa = 0$, while spectrum SDF2 has its maximum value at $\kappa = 0$. For both spectra, b is a correlation length parameter. Fig. 4 provides plots of SDF1 and SDF2 for different values of b and $\sigma_{gg} = 0.2$.

The underlying Gaussian field $g(x)$ is simulated according to SDF1 and SDF2 using the spectral representation method (e.g. [5]). Then the truncated Gaussian field $f_{\mathrm{TG}}(x)$ is obtained by simply truncating the simulated Gaussian field $g(x)$ in the following way: $-0.9 \leqslant g(x) \leqslant 0.9$, while the lognormal translation field $f_{\mathrm{L}}(x)$ and the triangular PDF translation field $f_{\mathrm{T}}(x)$ are obtained through the following non-linear transformations of Grigoriu's translation process theory (e.g. [2]):

$$f_{\mathrm{L}}(x) = F_{\mathrm{L}}^{-1}\{G[g(x)]\} \tag{31}$$

and

$$f_{\mathrm{T}}(x) = F_{\mathrm{T}}^{-1}\{G[g(x)]\}, \tag{32}$$

where F_{L}, F_{T}, and G denote the cumulative probability distribution functions of the lognormal, triangular and Gaussian distributions, respectively.

Because the simulated non-Gaussian fields $f_{\mathrm{TG}}(x)$, $f_{\mathrm{L}}(x)$ and $f_{\mathrm{T}}(x)$ used in the brute-force Monte Carlo simulations are obtained as non-linear transformations of the underlying Gaussian field $g(x)$ with prescribed spectral density function SDF1 or SDF2, their spectral density functions $S_{f_{\mathrm{TG}}f_{\mathrm{TG}}}(\kappa)$, $S_{f_{\mathrm{L}}f_{\mathrm{L}}}(\kappa)$ and $S_{f_{\mathrm{T}}f_{\mathrm{T}}}(\kappa)$ will be different from SDF1 and SDF2. These spectral density functions are however necessary in order to estimate $\mathrm{Var}[u(x)]$ using the integral form in Eq. (24). They are computed using the following formula:

$$S_{f_i f_i}(\kappa) = \frac{1}{2\pi L_x}\left|\int_0^{L_x} f_i(x)\mathrm{e}^{-\mathrm{i}\kappa x}\,\mathrm{d}x\right|^2; \quad i = \mathrm{TG},\ \mathrm{L},\ \text{or}\ \mathrm{T} \tag{33}$$

where L_x is the length of the sample functions of the non-Gaussian fields modeling the inverse of the elastic modulus. The $S_{ff}(\kappa)$ used in Eq. (24) is eventually determined by ensemble averaging.

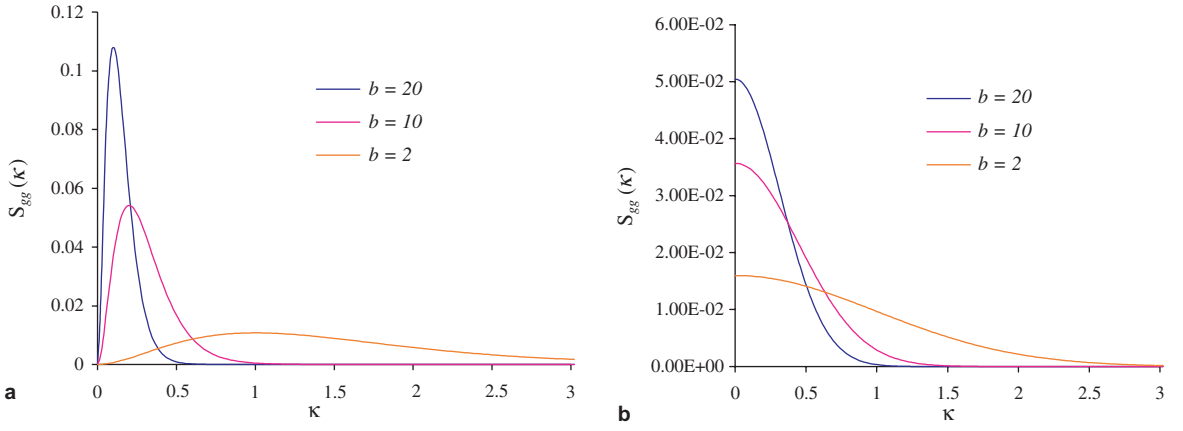

Fig. 4. (a) Spectral density function SDF1 plotted for three different values of the correlation length parameter b and $\sigma_{gg} = 0.2$. (b) Spectral density function SDF2 plotted for three different values of the correlation length parameter b and $\sigma_{gg} = 0.2$.

For the truncated Gaussian field, $\mathrm{Var}[u(x = L/2)]$ is computed through brute-force Monte Carlo simulations for various values of the correlation length parameter b in SDF1 and SDF2, and five different values of the standard deviation σ_{gg} of the underlying Gaussian field $g(x)$: $\sigma_{gg} = 0.2$, $\sigma_{gg} = 0.4$, $\sigma_{gg} = 0.6$, $\sigma_{gg} = 0.8$ and $\sigma_{gg} = 1.0$. The corresponding standard deviations of the truncated Gaussian field $f_{\mathrm{TG}}(x)$ are estimated as: $\sigma_{f_{\mathrm{TG}}f_{\mathrm{TG}}} = 0.2$, $\sigma_{f_{\mathrm{TG}}f_{\mathrm{TG}}} = 0.3925$, $\sigma_{f_{\mathrm{TG}}f_{\mathrm{TG}}} = 0.5313$, $\sigma_{f_{\mathrm{TG}}f_{\mathrm{TG}}} = 0.6184$ and $\sigma_{f_{\mathrm{TG}}f_{\mathrm{TG}}} = 0.675$, respectively. $\mathrm{Var}[u(x = L/2)]$ is also computed via the integration in Eq. (24) in conjunction with the FMCS procedure to estimate the variability response function. This computation is carried out with a sufficiently refined discretization of the integrand in Eq. (24) to achieve a sufficiently high level of accuracy. Fig. 5(a) provides plots of $\mathrm{Var}[u(x = L/2)]$ as a function of $\sigma_{f_{\mathrm{TG}}f_{\mathrm{TG}}}$ when SDF1 is used as the spectral density function of the underlying Gaussian field $g(x)$. Three different values of the correlation length parameter b are considered. Fig. 5(b) presents similar results for SDF2. Fig. 5(a) and (b) demonstrates that the values of $\mathrm{Var}[u(x = L/2)]$ computed using the integration in Eq. (24) and through brute-force Monte Carlo simulations practically coincide, regardless of the value of the standard deviation used for modeling the inverse of the modulus of elasticity.

The evolution of the relative error between the values of $\mathrm{Var}[u(x = L/2)]$ computed using the aforementioned two approaches is demonstrated in Fig. 6, by selecting two of the cases displayed in Fig. 5. Specifically, Fig. 6(a) presents the evolution of this error for SDF1 with $b = 2$ and $\sigma_{f_{\mathrm{TG}}f_{\mathrm{TG}}} = 0.6184$, while Fig. 6(b) presents corresponding results for SDF2 with the same values for b and $\sigma_{f_{\mathrm{TG}}f_{\mathrm{TG}}}$. The evolution of the relative error is plotted as a function of the number of samples in the brute-force Monte Carlo simulations (denoted by N_{samp}). Fig. 6(a) and (b) clearly indicates that the relative error approaches zero. Similar behavior of the relative error was observed in all cases considered. It is therefore claimed that the results of the aforementioned two approaches are identical in all cases considered in this study.

The same procedure is followed for the translation fields with lognormal and triangular PDFs. $\mathrm{Var}[u(x = L/2)]$ is again computed through brute-force Monte Carlo simulations using an underlying Gaussian field with spectral density functions SDF1 and SDF2. Different values are considered for the

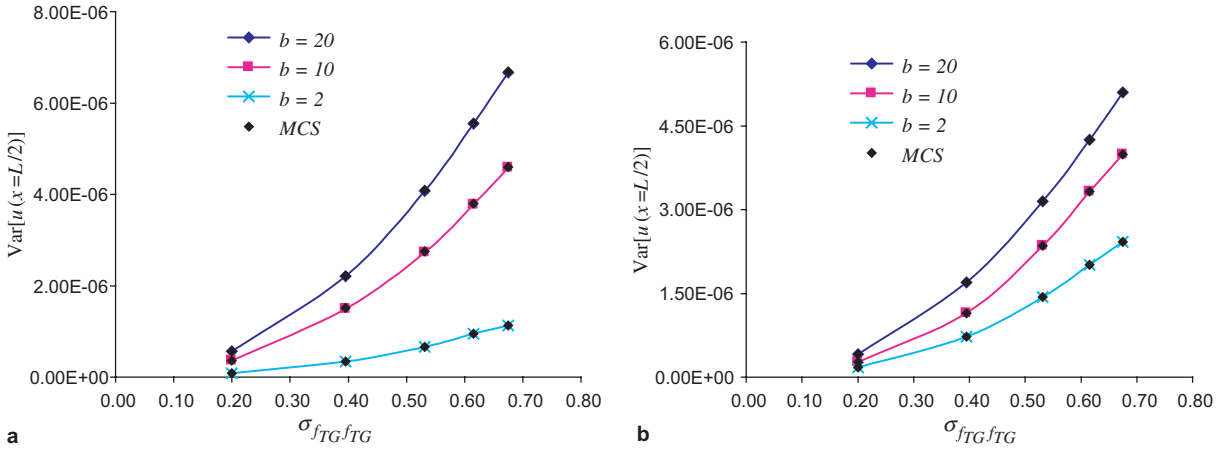

Fig. 5. (a) Variance of response displacement at $x = L/2$ for the beam shown in Fig. 2 as a function of the standard deviation $\sigma_{f_{\mathrm{TG}}f_{\mathrm{TG}}}$: Comparison of results from the integration of Eq. (24) and from brute-force Monte Carlo simulations (MCS). Plots correspond to three different values of correlation length parameter b of spectral density function SDF1. The corresponding PDF is a truncated Gaussian. (b) Variance of response displacement at $x = L/2$ for the beam shown in Fig. 2 as a function of the standard deviation $\sigma_{f_{\mathrm{TG}}f_{\mathrm{TG}}}$: Comparison of results from the integration of Eq. (24) and from brute-force Monte Carlo simulations (MCS). Plots correspond to three different values of correlation length parameter b of spectral density function SDF2. The corresponding PDF is a truncated Gaussian.

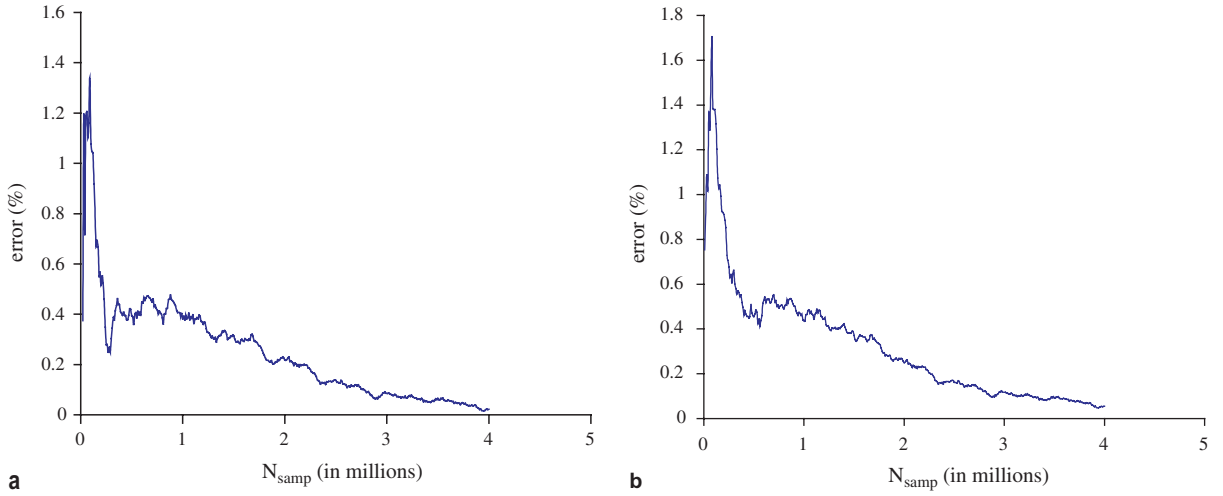

Fig. 6. (a) Evolution of relative error for SDF1 with $b = 2$ and $\sigma_{f_{TG}f_{TG}} = 0.6184$. (b) Evolution of relative error for SDF2 with $b = 2$ and $\sigma_{f_{TG}f_{TG}} = 0.6184$.

correlation length parameter b. Four different values are considered for the standard deviations $\sigma_{f_L f_L}$ and $\sigma_{f_T f_T}$ of stochastic fields $f_L(x)$ and $f_T(x)$ respectively. They are displayed in Tables 1 and 2 together with the corresponding lower limits of the lognormal and triangular PDFs. Var$[u(x = L/2)]$ is also computed via the integration in Eq. (24) in conjunction with the FMCS procedure to estimate the variability response function. Fig. 7(a) provides plots of Var$[u(x = L/2)]$ as a function of $\sigma_{f_L f_L}$ for the case of the lognormal translation field, while Fig. 7(b) presents similar results for the case of the translation field with triangular PDF. As with Figs. 5(a) and 5(b), Figs. 7(a) and 7(b) demonstrate again that the values of Var$[u(x = L/2)]$ computed using the integration in Eq. (24) and through brute-force Monte Carlo simulations practically coincide, regardless of the value of the standard deviation used for modeling the inverse of the modulus of elasticity. As mentioned above, the evolution of the relative error in these two cases (lognormal and triangular PDF's) is similar to that of the truncated Gaussian field (refer to Fig. 6).

The validity of the two assumptions of existence and independence (that have been considered to form a conjecture) has been demonstrated numerically in this section for a wide range of stochastic fields $f(x)$. Although such a numerical demonstration does not constitute a formal mathematical proof, the results displayed in Figs. 5 and 7 provide "very strong numerical evidence" for the validity of the conjecture.

Table 1
Values of standard deviation $\sigma_{f_L f_L}$ considered and corresponding lower bounds of the lognormal PDF

$\sigma_{f_L f_L}$	0.2	0.4	0.6	0.7
Lower limit	−0.40	−0.60	−0.80	−0.95

Table 2
Values of standard deviation $\sigma_{f_T f_T}$ considered and corresponding lower bounds of the triangular PDF

$\sigma_{f_T f_T}$	0.20	0.40	0.60	0.70
Lower limit	−0.28	−0.56	−0.85	−0.99

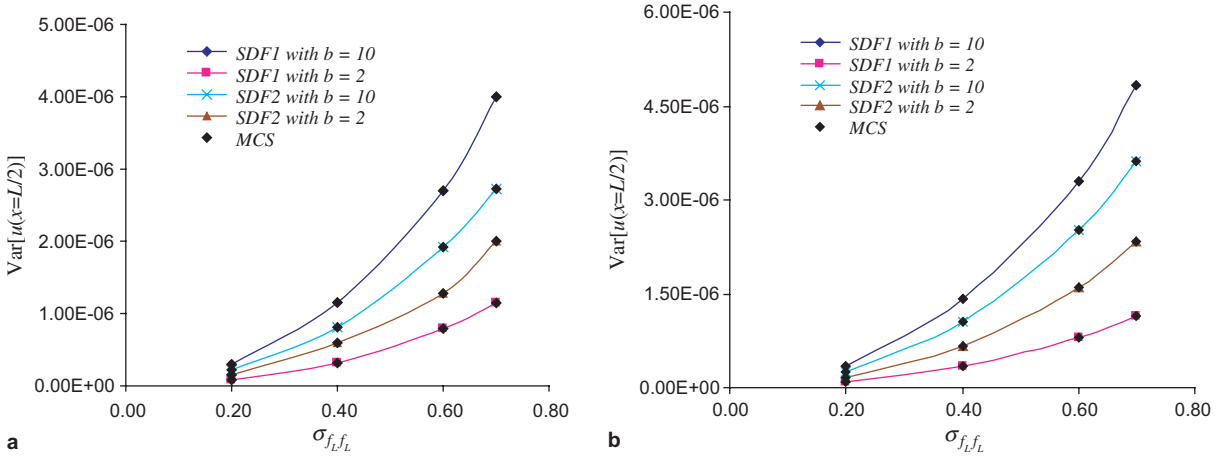

Fig. 7. (a) Variance of response displacement at $x = L/2$ for the beam shown in Fig. 2 as a function of the standard deviation $\sigma_{f_L f_L}$: Comparison of results from the integration of Eq. (24) and from brute-force Monte Carlo simulations (MCS). Plots correspond to two values of correlation length parameter b of spectral density functions SDF1 and SDF2. The corresponding PDF is a lognormal. (b) Variance of response displacement at $x = L/2$ for the beam shown in Fig. 2 as a function of the standard deviation $\sigma_{f_T f_T}$: Comparison of results from the integration of Eq. (24) and from brute-force Monte Carlo simulations (MCS). Plots correspond to two values of correlation length parameter b of spectral density functions SDF1 and SDF2. The corresponding PDF is triangular.

3.2.2. Limitation in FMCS procedure

The following limitation is implied when the Fast Monte Carlo Simulation procedure is used to estimate the variability response function: as the flexibility cannot become negative at any point of the structure, the standard deviation σ_{ff} of the random sinusoids modeling the inverse of the elastic modulus cannot exceed the value of $1/\sqrt{2}$ (refer to Eq. (27)). For values greater than this limit, FMCS cannot be applied in the form presented in this paper, as this will result in negative values of the flexibility. Although extending the applicability of FMCS beyond this limiting value of σ_{ff} is beyond the scope of this paper, the following general concept is provided here: it is believed that for values of σ_{ff} larger than $1/\sqrt{2}$, the random sinusoid should be replaced with a zero mean field taking only positive values and having a spectral density function as close as possible to the delta-function SDF of the corresponding random sinusoid (at the desired wave number). The full development of this concept is the subject of future research.

3.2.3. Closed-form expression for the variability response function in Eq. (26)

An important consequence of the validity of the two assumptions mentioned in the previous section is that the VRF(x, κ, σ_{ff}) in Eq. (26) can be computed using the fast Monte Carlo simulation (FMCS) approach described earlier. There is no need therefore for establishing closed-form analytic expressions for $A^*(x, \kappa)$, $A^{**}(x, \kappa)$ and $A^{***}(x, \kappa)$ in Eq. (26). Although this is true, it will be demonstrated now how to obtain such closed-form analytic expressions in order to show that the VRF(x, κ, σ_{ff}) is indeed a function of σ_{ff} as claimed earlier and as demonstrated numerically in Fig. 3.

To accomplish this, Eq. (22) is rewritten in the following way:

$$R_{fp}(x_1, x_2) = \int_{-\infty}^{\infty} B(x_1, x_2, \kappa) S_{ff}(\kappa)\, \mathrm{d}\kappa, \tag{34}$$

where

$$B(x_1, x_2, \kappa) = A^{**}(x_2, \kappa)\cos[\kappa(x_2 - x_1)] + A^{***}(x_2, \kappa)\sin[\kappa(x_2 - x_1)] \tag{35}$$

is an even function of κ.

Closed-form analytic expressions for $A^*(x,\kappa)$ and $B(x_1,x_2,\kappa)$ can be obtained now by assuming that stochastic field $f(x)$ in Eqs. (17) and (34) becomes a random sinusoid at wave number $\bar{\kappa}$:

$$f(x) = \sqrt{2}\sigma_{ff}\cos(\bar{\kappa}x + \phi) \tag{36}$$

with corresponding spectral density function a delta function at $\bar{\kappa}$:

$$S_{ff}(\kappa) = \sigma_{ff}^2\delta(\kappa - \bar{\kappa}). \tag{37}$$

This operation on Eqs. (17) and (34) yields the following expressions for $\kappa = \bar{\kappa}$:

$$A^*(x_1,\kappa)A^*(x_2,\kappa) = \frac{1}{\sigma_{ff}^2}\frac{[R_{pp}(x_1,x_2)]_\kappa}{e^{i\kappa(x_1-x_2)}}, \tag{38}$$

$$B(x_1,x_2,\kappa) = \frac{1}{\sigma_{ff}^2}[R_{fp}(x_1,x_2)]_\kappa, \tag{39}$$

where $[R_{pp}(x_1,x_2)]_\kappa$ and $[R_{fp}(x_1,x_2)]_\kappa$ denote the autocorrelation and cross-correlation functions $R_{pp}(x_1,x_2)$ and $R_{fp}(x_1,x_2)$ evaluated when stochastic field $f(x)$ becomes a random sinusoid. Considering the expressions in Eqs. (36) and (11), it is straightforward to show that:

$$A^*(x,\kappa) = \frac{1}{\sigma_{ff}}\left\{\varepsilon[R_\kappa^2(1+\sqrt{2}\sigma_{ff}\cos(\kappa x+\phi))^2] - \varepsilon[R_\kappa(1+\sqrt{2}\sigma_{ff}\cos(\kappa x+\phi))]^2\right\}, \tag{40}$$

$$B(x_1,x_2,\kappa) = \frac{1}{\sigma_{ff}^2}\left\{\varepsilon[R_\kappa\sqrt{2}\sigma_{ff}\cos(\kappa x_1+\phi)] + \varepsilon[2R_\kappa\sigma_{ff}^2\cos(\kappa x_1+\phi)\cos(\kappa x_2+\phi)]\right\}, \tag{41}$$

where R_κ denotes the redundant force defined in Eq. (8) for the particular case considered here involving stochastic field $f(x)$ as a random sinusoid:

$$R_\kappa = \frac{\frac{Q_0}{2}\int_0^L (L-\xi)^3(1+\sqrt{2}\sigma_{ff}\cos(\kappa\xi+\phi))\,d\xi}{\int_0^L (L-\xi)^2(1+\sqrt{2}\sigma_{ff}\cos(\kappa\xi+\phi))\,d\xi}. \tag{42}$$

The only uncertain quantity involved in the expectations shown in Eqs. (40) and (41) is the random phase angle ϕ that is uniformly distributed in the range $[0,2\pi]$. It is therefore possible to establish closed-form analytic expressions for $A^*(x,\kappa)$ and $B(x_1,x_2,\kappa)$ using any symbolic algebra software. The resulting expressions are very complicated and for this reason are not provided here. However, it is obvious that the resulting expressions for $A^*(x,\kappa)$ and $B(x_1,x_2,\kappa)$ will be functions of the standard deviation σ_{ff} of stochastic field $f(x)$ and of the (deterministic) geometry, loading and boundary conditions of the beam (note that the expressions for $A^*(x,\kappa)$ and $B(x_1,x_2,\kappa)$ will be independent of the random phase angle ϕ, since the evaluation of the expectations in Eqs. (40) and (41) involves integration with respect to ϕ). Finally, it should be mentioned that the establishment of Eqs. (38)–(41) is based on the assumption that $A^*(x,\kappa)$ and $B(x_1,x_2,\kappa)$ are independent from $S_{ff}(\kappa)$.

3.3. Generality of integral expression in Eq. (24)

Whether the variability response function (VRF) is computed from the closed-form expressions in Eqs. (26), (35), (40) and (41), or using the fast Monte Carlo simulation (FMCS) approach, it should be mentioned that there were no first-order approximations made whatsoever. Furthermore, similar closed-form expressions can be established in principle for any statically indeterminate beam/frame with any kind of boundary and loading conditions, as far as it can be analysed using a flexibility-based formulation similar to the one in Eq. (6) (with no limitation in the number of redundant forces). As such closed-form expres-

sions for the VRF become exceedingly complicated as the number of redundant forces increases, the VRF is usually computed using the FMCS approach.

4. Upper bounds on response variability

Using Eq. (4), upper bounds on the response displacement variance of a statically determinate beam can be established in a straightforward way as follows:

$$\mathrm{Var}[u(x)] = \int_{-\infty}^{\infty} \mathrm{VRF}(x,\kappa) S_{ff}(\kappa)\,\mathrm{d}\kappa \leqslant \mathrm{VRF}(x,\kappa^{\max})\sigma_{ff}^2, \tag{43}$$

where $\kappa^{\max}$ is the wave number at which the VRF takes its maximum value, and σ_{ff}^2 is the variance of stochastic field $f(x)$ modeling the inverse of the elastic modulus. Eq. (24) is used to determine the corresponding bounds for statically indeterminate beams:

$$\mathrm{Var}[u(x)] = \int_{-\infty}^{\infty} \mathrm{VRF}(x,\kappa,\sigma_{ff}) S_{ff}(\kappa)\,\mathrm{d}\kappa \leqslant \mathrm{VRF}(x,\kappa^{\max},\sigma_{ff})\sigma_{ff}^2, \tag{44}$$

where $\kappa^{\max}$ is the wave number at which the VRF corresponding to a given value of σ_{ff} takes its maximum value, and σ_{ff}^2 is the variance of stochastic field $f(x)$ modeling the inverse of the elastic modulus.

The upper bounds shown in Eqs. (43) and (44) are physically realizable since the form of stochastic field $f(x)$ that produces them is known. Specifically, the variance of $u(x)$ attains its maximum value when random field $f(x)$ becomes a random sinusoid:

$$f(x) = \sqrt{2}\sigma_{ff}\cos(\kappa^{\max}x + \phi), \tag{45}$$

where ϕ is a random phase angle uniformly distributed in $[0, 2\pi]$. In this case, the corresponding spectral density function of $f(x)$ is a delta function at wave number $\kappa^{\max}$:

$$S_{ff}(\kappa) = \sigma_{ff}^2\delta(\kappa - \kappa^{\max}), \tag{46}$$

while its PDF is a beta probability distribution function given by:

$$p_f(s) = \frac{1}{\pi\sqrt{2\sigma_{ff}^2 - s^2}} \quad \text{with } -\sqrt{2}\sigma_{ff} \leqslant s \leqslant \sqrt{2}\sigma_{ff}. \tag{47}$$

The upper bounds shown in Eqs. (43) and (44) are spectral- and probability-distribution-free, as the only probabilistic parameter they depend on is the standard deviation of the inverse of the elastic modulus.

4.1. Bound generating fields

The concept of bound generating fields was introduced in [3]. It is summarized here as it will be used later in the numerical examples section.

Whether a statically determinate or indeterminate beam is considered, the variance of the response displacement attains its maximum value when random field $f(x)$ becomes a random sinusoid (Eq. (45)). Consequently, the following expression can be written for the inverse of the elastic modulus that produces the upper bounds:

$$\frac{1}{E(x)} = F_0[1 + f(x)] = F_0[1 + \sqrt{2}\sigma_{ff}\cos(\kappa^{\max}x + \phi)]. \tag{48}$$

A new stochastic field $f^*(x)$ modeling the elastic modulus and corresponding to stochastic field $f(x)$ modeling the inverse of the elastic modulus can be defined now for this case that produces the upper bounds:

$$E(x) = \frac{1}{F_0}\frac{1}{[1+f(x)]} = E_0[1+f^*(x)], \tag{49}$$

where E_0 is the mean value of the elastic modulus which is related to F_0 via:

$$E_0 = \frac{1}{F_0}\varepsilon\left[\frac{1}{(1+f(x))}\right] \tag{50}$$

$f^*(x)$ is a zero-mean, homogeneous stochastic field related to $f(x)$ through the following relationship:

$$f^*(x) = \frac{1-\varepsilon\left[\frac{1}{(1+f(x))}\right](1+f(x))}{\varepsilon\left[\frac{1}{(1+f(x))}\right](1+f(x))}. \tag{51}$$

Stochastic field $f^*(x)$ is called a bound generating field (BGF) since it produces realizable upper bounds. Sample functions of $f^*(x)$ can be easily obtained from generated realizations of the random sinusoid $f(x)$ using Eq. (51). A closed-form analytic expression for the PDF of $f^*(x)$ is available, and its spectral density function can be easily estimated from generated sample functions of $f^*(x)$ (refer to [3] for a detailed description of BGFs and their properties).

4.2. Three alternative ways to perform fast Monte Carlo simulation

Eq. (51) indicates that when random field $f(x)$ modeling the inverse of the elastic modulus is a random sinusoid, random field $f^*(x)$ modeling the elastic modulus can be fully determined, i.e. a sample function of $f^*(x)$ can be computed from a given sample function of $f(x)$. Consequently, there are essentially three alternative ways to perform the fast Monte Carlo simulation to estimate $\mathrm{Var}[u(x)]_{\bar{\kappa}}$ in Eq. (28):

1. By generating sample functions of $f(x)$ (in this case a random sinusoid) and then using a closed-form analytic expression for the response displacement (Eq. (7)). This approach is called $ANA - f(x)$.
2. By generating sample functions of $f(x)$ (in this case a random sinusoid), computing the corresponding sample functions of $f^*(x)$ using Eq. (51), and then using a closed-form analytic expression for the response displacement. This approach is called $ANA - f^*(x)$.
3. By generating sample functions of $f(x)$ (in this case a random sinusoid), computing the corresponding sample functions of $f^*(x)$ using Eq. (51), and then using a deterministic finite element code to estimate the response displacement. This approach is called $FEM - f^*(x)$.

It is obvious that the third approach is not requiring the existence of a closed-form analytic expression for the response displacement. All three approaches provide identical estimates of $\mathrm{Var}[u(x)]_{\bar{\kappa}}$ (and consequently of the variability response function too).

At this juncture, it should be mentioned that although in the case of statically determinate beams the variability response function can be computed from the closed-form analytic expression shown in Eq. (5), alternatively, the $\mathrm{VRF}(x,\kappa)$ can also be estimated using the fast Monte Carlo simulation approach described earlier for statically indeterminate beams. This is very helpful in cases where function $g(x,\xi)$ of the statically determinate problem becomes too cumbersome.

5. Numerical examples

Example 1. Consider again the fixed-simply supported beam of length $L = 10$ m shown in Fig. 2. Two load cases are considered: LC1 consisting of a uniformly distributed load $Q_0 = 1000$ N/m and LC2 consisting of

the same uniformly distributed load $Q_0 = 1000$ N/m and a concentrated moment $M_0 = -10{,}000$ Nm applied at its right end (please note that this concentrated moment is not indicated in Fig. 2). All loads are assumed again to be deterministic. The inverse of the elastic modulus of the beam is assumed to vary randomly along its length according to Eq. (1) with $F_0 = 8 \times 10^{-9}$ m^2/N and $I = 0.1$ m^4.

5.1. Analysis of response variability

For LC1, an extensive numerical investigation was performed in section "*Demonstration of the validity of the assumptions of existence and independence*" where Var$[u(x = L/2)]$ was estimated using the integration in Eq. (24) in conjunction with the $ANA - f(x)$ technique for calculating the VRF, and through brute-force Monte Carlo simulations. As can be observed in Figs. 5–7, the two approaches produced practically identical results in all cases considered.

The same procedure is followed now for LC2. Fig. 8 displays plots of VRF$(x = 3L/4, \kappa, \sigma_{ff})$ calculated using the $ANA - f(x)$ approach for various values of the standard deviation σ_{ff}. As with LC1 (Fig. 3), Fig. 8 indicates that the VRF of LC2 is again a function of the standard deviation σ_{ff}, while the differences observed among the different VRF curves obtained for the four values of σ_{ff} considered are relatively small (and become negligible for $\sigma_{ff} < 0.4$). Numerical results for LC2 are obtained for a truncated Gaussian field only (having the same definition as before). Fig. 9 provides plots of Var$[u(x = 3L/4)]$ as a function of $\sigma_{f_{TG}f_{TG}}$ when SDF1 and SDF2 are used as the spectral density function of the underlying Gaussian field $g(x)$. Two different values of the correlation length parameter b are considered. Fig. 9 indicates that the values of Var$[u(x = 3L/4)]$ computed using the integration in Eq. (24) and through brute-force Monte Carlo simulations practically coincide, regardless of the value of the standard deviation used for modeling the inverse of the modulus of elasticity. The evolution of the relative error for LC2 is similar to that shown in Fig. 6.

The variance of the response displacement can be calculated with minimal computational effort using the integration in Eq. (24) for prescribed forms of the spectral density function $S_{ff}(\kappa)$. Fig. 10(a) and (b) displays results of such calculations for LC1 and LC2 respectively. SDF1 and SDF2 are used to model $S_{ff}(\kappa)$ with standard deviation $\sigma_{ff} = 0.4$. The computed results are plotted as a function of correlation distance parameter b.

5.1.1. Spectral- and probability-distribution-free upper bounds

Spectral- and probability-distribution-free upper bounds for the variance of the response displacement are computed now using Eq. (44). For LC1, upper bounds are determined for Var$[u(x = L/2)]$ for various values of the standard deviation σ_{ff} of the inverse of the elastic modulus:

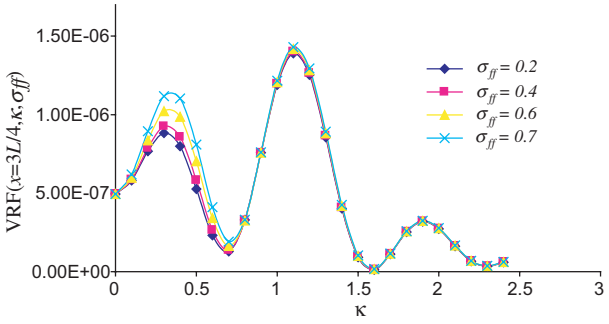

Fig. 8. Variability response function calculated using the FMCS approach for the beam in Example 1 and for LC2. Four different values σ_{ff} are considered.

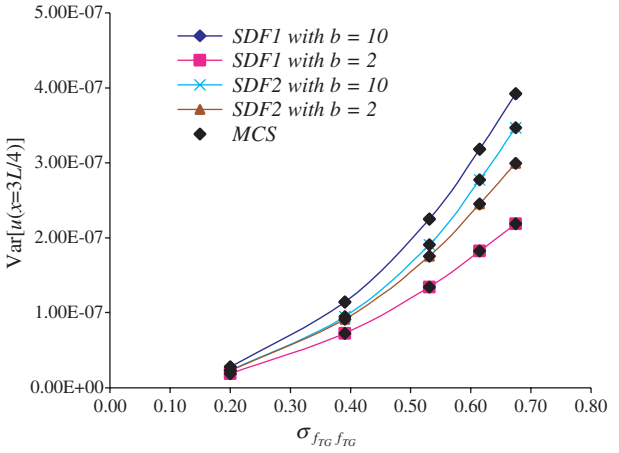

Fig. 9. Example 1 and LC2: Variance of response displacement at $x = 3L/4$ as a function of standard deviation $\sigma_{f_{TG}f_{TG}}$: Comparison of results from the integration of Eq. (24) and from brute-force Monte Carlo simulations (MCS). Plots correspond to two values of correlation length parameter b of spectral density functions SDF1 and SDF2. The corresponding PDF is a truncated Gaussian.

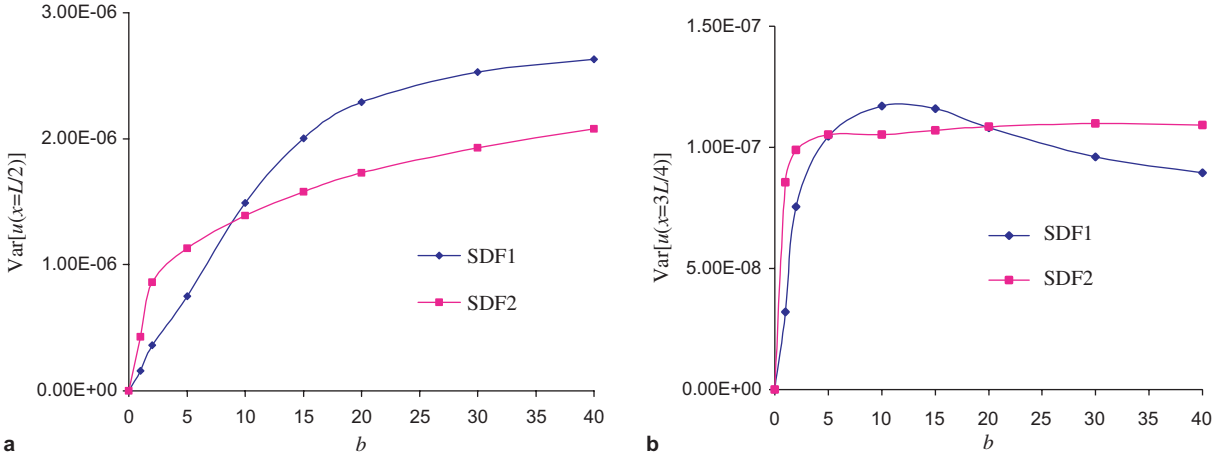

Fig. 10. (a) Example 1 and LC1: Variance of response displacement at $x = L/2$ calculated through the integration in Eq. (24) and using SDF1 and SDF2 to model the spectral density function $S_{ff}(\kappa)$. Both curves are established for $\sigma_{ff} = 0.4$ and plotted as a function of correlation length parameter b. (b) Example 1 and LC2: Variance of response displacement at $x = L/2$ calculated through the integration in Eq. (24) and using SDF1 and SDF2 to model the spectral density function $S_{ff}(\kappa)$. Both curves are established for $\sigma_{ff} = 0.4$ and plotted as a function of correlation length parameter b.

$$\mathrm{Var}[u(x = L/2)] \leqslant \mathrm{VRF}(x = L/2, \kappa^{\max}, \sigma_{ff} = 0.2) \cdot 0.2^2 = 7.00 \times 10^{-7}; \quad \kappa^{\max} = 0, \tag{52}$$

$$\mathrm{Var}[u(x = L/2)] \leqslant \mathrm{VRF}(x = L/2, \kappa^{\max}, \sigma_{ff} = 0.4) \cdot 0.4^2 = 2.78 \times 10^{-6}; \quad \kappa^{\max} = 0, \tag{53}$$

$$\mathrm{Var}[u(x = L/2)] \leqslant \mathrm{VRF}(x = L/2, \kappa^{\max}, \sigma_{ff} = 0.6) \cdot 0.6^2 = 6.26 \times 10^{-6}; \quad \kappa^{\max} = 0, \tag{54}$$

$$\mathrm{Var}[u(x = L/2)] \leqslant \mathrm{VRF}(x = L/2, \kappa^{\max}, \sigma_{ff} = 0.7) \cdot 0.7^2 = 8.53 \times 10^{-6}; \quad \kappa^{\max} = 0. \tag{55}$$

For LC2, upper bounds are determined for $\mathrm{Var}[u(x = 3L/4)]$:

$$\mathrm{Var}[u(x = 3L/4)] \leqslant \mathrm{VRF}(x = 3L/4, \kappa^{\max}, \sigma_{ff} = 0.2) \cdot 0.2^2 = 5.56 \times 10^{-8}; \quad \kappa^{\max} = 1.1, \tag{56}$$

$$\mathrm{Var}[u(x = 3L/4)] \leqslant \mathrm{VRF}(x = 3L/4, \kappa^{\max}, \sigma_{ff} = 0.4) \cdot 0.4^2 = 2.24 \times 10^{-7}; \quad \kappa^{\max} = 1.1, \tag{57}$$

$$\mathrm{Var}[u(x = 3L/4)] \leqslant \mathrm{VRF}(x = 3L/4, \kappa^{\max}, \sigma_{ff} = 0.6) \cdot 0.6^2 = 5.09 \times 10^{-7}; \quad \kappa^{\max} = 1.1, \tag{58}$$

$$\mathrm{Var}[u(x = 3L/4)] \leqslant \mathrm{VRF}(x = 3L/4, \kappa^{\max}, \sigma_{ff} = 0.7) \cdot 0.7^2 = 7.01 \times 10^{-7}; \quad \kappa^{\max} = 1.1. \tag{59}$$

For LC1, the upper bounds shown in Eqs. (52)–(55) are obtained when stochastic field $f(x)$ modeling the inverse of the elastic modulus degenerates into a random variable (as $\kappa^{\max} = 0$). For LC2, the upper bounds shown in Eqs. (56)–(59) are obtained when stochastic field $f(x)$ becomes a random sinusoid with wave number $\kappa^{\max} = 1.1$. In this case, the bound generating field $f^*(x)$ modelling the elastic modulus can be easily determined from Eq. (51).

Example 2. Consider now the twice-statically-indeterminate fixed beam of length $L = 10$ m shown in Fig. 11. Two load cases are considered in this example: LC1 consisting of a concentrated force $P_0 = 10{,}000$ N acting at the midspan ($x = L/2$), and LC2 consisting of the same concentrated force $P_0 = 10{,}000$ N and a concentrated moment $M_0 = 10{,}000$ N m acting also at $x = L/2$ (please note that this concentrated moment is not indicated in Fig. 2). All loads are assumed again to be deterministic. The inverse of the elastic modulus of the beam is assumed to vary randomly along its length according to Eq. (1) with $F_0 = 8 \times 10^{-9}$ m^2/N and $I = 0.1$ m^4.

5.2. Analysis of response variability

The same procedure as in Example 1 is followed here. Fig. 12 displays plots of $\mathrm{VRF}(x = 3L/4, \kappa, \sigma_{ff})$ calculated using the $FEM - f^*(x)$ approach for LC1, while Fig. 13 displays similar plots for LC2. For the

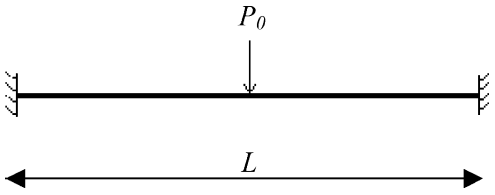

Fig. 11. Configuration of fixed statically indeterminate beam.

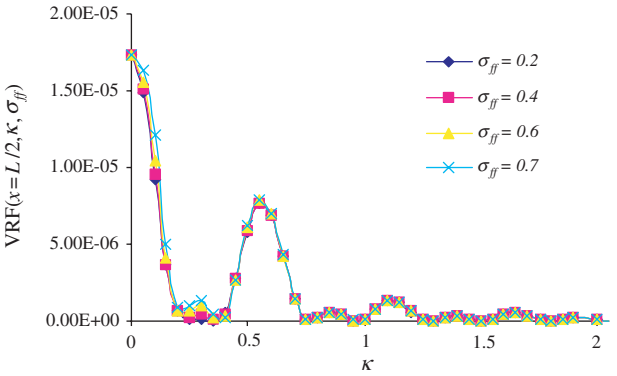

Fig. 12. Variability response function calculated using the FMCS approach for the beam in Example 2 and for LC1. Four different values σ_{ff} are considered.

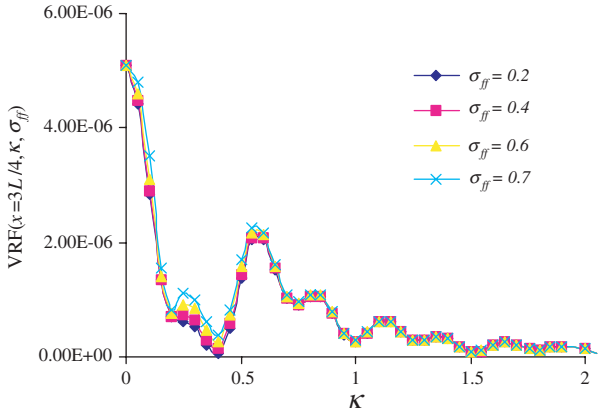

Fig. 13. Variability response function calculated using the FMCS approach for the beam in Example 2 and for LC2. Four different values σ_{ff} are considered.

FEM analysis, the beam is discretized into 100 finite elements. As in Example 1, Figs. 12 and 13 indicate that the VRF is again a function of σ_{ff}, while the differences observed among the four VRF curves obtained for the four values of σ_{ff} considered are relatively small (and become negligible for $\sigma_{ff} < 0.4$). In this example, only the truncated Gaussian field is considered (having the same definition as before). Fig. 14 provides plots of $\mathrm{Var}[u(x = L/2)]$ for LC1 as a function of $\sigma_{f_{\mathrm{TG}} f_{\mathrm{TG}}}$ when SDF1 and SDF2 are used as the spectral density function of the underlying Gaussian field $g(x)$. Two different values of the correlation length parameter b are considered. Fig. 15 provides similar plots for $\mathrm{Var}[u(x = 3L/4)]$ and LC2. Figs. 14 and 15 indicate that the values for the variance of the response displacement computed using the integration in Eq. (24) and through brute-force Monte Carlo simulations practically coincide, regardless of the value of the standard deviation used for modeling the inverse of the modulus of elasticity. The evolution of the relative error for both LC1 and LC2 is similar to that shown in Fig. 6.

Fig. 16(a) and (b) displays results for $\mathrm{Var}[u(x = L/2)]$ and $\mathrm{Var}[u(x = 3L/4)]$ corresponding to LC1 and LC2, respectively, calculated using the integration in Eq. (24). SDF1 and SDF2 are used to model $S_{ff}(\kappa)$

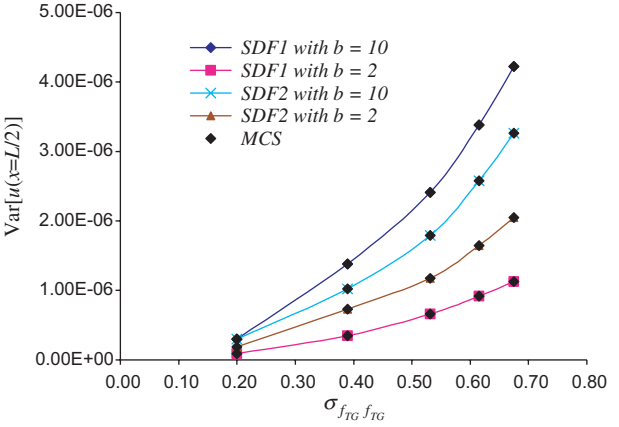

Fig. 14. Example 2 and LC1: Variance of response displacement at $x = L/2$ as a function of standard deviation $\sigma_{f_{\mathrm{TG}} f_{\mathrm{TG}}}$: Comparison of results from the integration of Eq. (24) and from brute-force Monte Carlo simulations (MCS). Plots correspond to two values of correlation length parameter b of spectral density functions SDF1 and SDF2. The corresponding PDF is a truncated Gaussian.

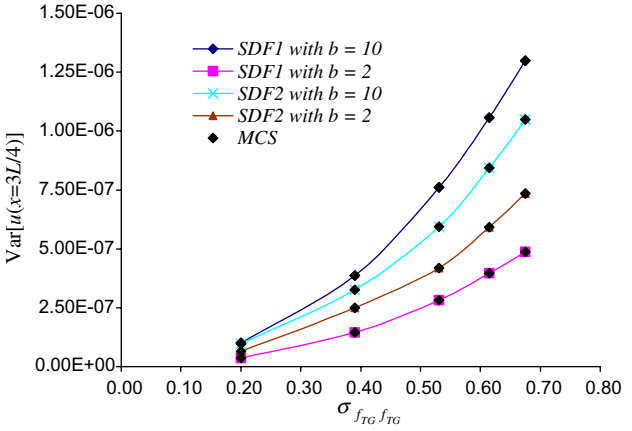

Fig. 15. Example 2 and LC2: Variance of response displacement at $x = 3L/4$ as a function of standard deviation $\sigma_{f_{TG}f_{TG}}$: Comparison of results from the integration of Eq. (24) and from brute-force Monte Carlo simulations (MCS). Plots correspond to two values of correlation length parameter b of spectral density functions SDF1 and SDF2. The corresponding PDF is a truncated Gaussian.

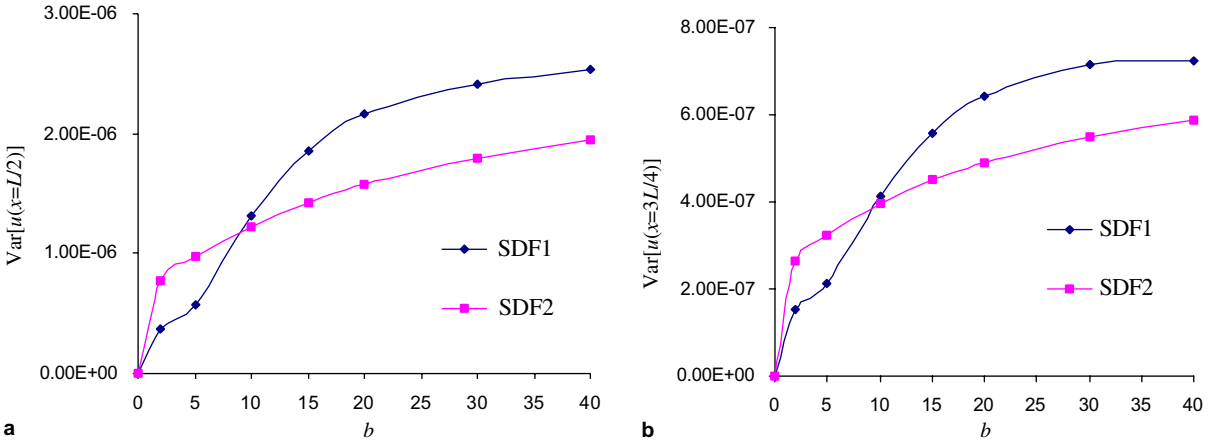

Fig. 16. (a) Example 2 and LC1: Variance of response displacement at $x = L/2$ calculated through the integration in Eq. (24) and using SDF1 and SDF2 to model the spectral density function $S_{ff}(\kappa)$. Both curves are established for $\sigma_{ff} = 0.4$ and plotted as a function of correlation length parameter b. (b) Example 2 and LC2: Variance of response displacement at $x = 3L/4$ calculated through the integration in Eq. (24) and using SDF1 and SDF2 to model the spectral density function $S_{ff}(\kappa)$. Both curves are established for $\sigma_{ff} = 0.4$ and plotted as a function of correlation length parameter b.

with standard deviation $\sigma_{ff} = 0.4$. The computed results are plotted as a function of correlation distance parameter b.

5.2.1. Spectral- and probability-distribution-free upper bounds

Spectral- and probability-distribution-free upper bounds for the variance of the response displacement are computed now using Eq. (44). For LC1, upper bounds are determined for $\mathrm{Var}[u(x = L/2)]$ for various values of the standard deviation σ_{ff} of the inverse of the elastic modulus:

$$\mathrm{Var}[u(x=L/2)] \leqslant \mathrm{VRF}(x=L/2,\kappa^{\max},\sigma_{ff}=0.2)\cdot 0.2^2 = 6.92\times 10^{-6};\quad \kappa^{\max}=0, \tag{60}$$

$$\mathrm{Var}[u(x=L/2)] \leqslant \mathrm{VRF}(x=L/2,\kappa^{\max},\sigma_{ff}=0.4)\cdot 0.4^2 = 2.77\times 10^{-6};\quad \kappa^{\max}=0, \tag{61}$$

$$\mathrm{Var}[u(x=L/2)] \leqslant \mathrm{VRF}(x=L/2,\kappa^{\max},\sigma_{ff}=0.6)\cdot 0.6^2 = 6.20\times 10^{-6};\quad \kappa^{\max}=0, \tag{62}$$

$$\mathrm{Var}[u(x=L/2)] \leqslant \mathrm{VRF}(x=L/2,\kappa^{\max},\sigma_{ff}=0.7)\cdot 0.7^2 = 8.48\times 10^{-6};\quad \kappa^{\max}=0. \tag{63}$$

For LC2, upper bounds are determined for $\mathrm{Var}[u(x=3L/4)]$:

$$\mathrm{Var}[u(x=3L/4)] \leqslant \mathrm{VRF}(x=3L/4,\kappa^{\max},\sigma_{ff}=0.2)\cdot 0.2^2 = 2.04\times 10^{-7};\quad \kappa^{\max}=0, \tag{64}$$

$$\mathrm{Var}[u(x=3L/4)] \leqslant \mathrm{VRF}(x=3L/4,\kappa^{\max},\sigma_{ff}=0.4)\cdot 0.4^2 = 8.16\times 10^{-7};\quad \kappa^{\max}=0, \tag{65}$$

$$\mathrm{Var}[u(x=3L/4)] \leqslant \mathrm{VRF}(x=3L/4,\kappa^{\max},\sigma_{ff}=0.6)\cdot 0.6^2 = 1.83\times 10^{-6};\quad \kappa^{\max}=0, \tag{66}$$

$$\mathrm{Var}[u(x=3L/4)] \leqslant \mathrm{VRF}(x=3L/4,\kappa^{\max},\sigma_{ff}=0.7)\cdot 0.7^2 = 2.50\times 10^{-6};\quad \kappa^{\max}=0. \tag{67}$$

For both LC1 and LC2, the upper bounds shown in Eqs. (60)–(67) are obtained when stochastic field $f(x)$ modeling the inverse of the elastic modulus degenerates into a random variable (as $\kappa^{\max}=0$).

Example 3. Consider finally the statically indeterminate portal plane frame shown in Fig. 17 with $L=4$ m. The two base nodes are assumed fixed against translations and rotations. The loading consists of a deterministic horizontal force equal to $P_0=10{,}000$ N applied at node A (refer to Fig. 17). The inverse of the elastic modulus of the frame is assumed to vary randomly along its length according to Eq. (1) with $F_0=8\times 10^{-9}$ m^2/N and $I=0.1$ m^4.

5.3. Analysis of response variability

The same procedure as in Examples 1 and 2 is also followed here. Denoting by $u_{\mathrm{A_h}}$ the horizontal displacement of node A and by $\mathrm{VRF}_{\mathrm{A_h}}(\kappa,\sigma_{ff})$ the corresponding variability response function, Fig. 18 displays plots of $\mathrm{VRF}_{\mathrm{A_h}}(\kappa,\sigma_{ff})$ calculated using the $FEM-f^*(x)$ approach. For the FEM analysis, the frame is discretized into 120 finite elements. As in Examples 1 and 2, Fig. 18 indicates that the VRF is again a function of σ_{ff}, while the differences observed among the four VRF curves obtained for the four values of σ_{ff} considered are relatively small (and become negligible for $\sigma_{ff}<0.4$). In this example, only the truncated Gaussian field is considered with SDF1 and $b=2$. Fig. 19 provides plots of $\mathrm{Var}(u_{\mathrm{A_h}})$ as a function of $\sigma_{f_{\mathrm{TG}}f_{\mathrm{TG}}}$. Fig. 19 indicates that the values for the variance of the response displacement computed using

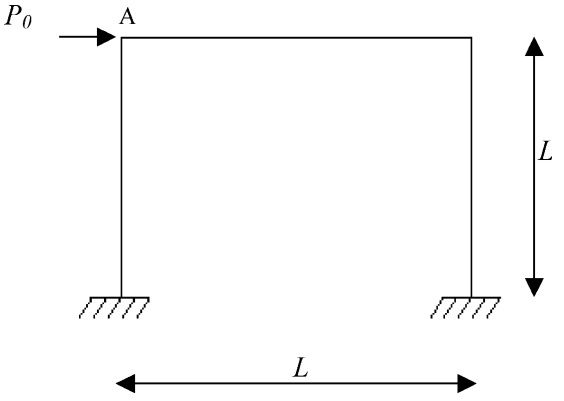

Fig. 17. Portal frame considered in Example 3.

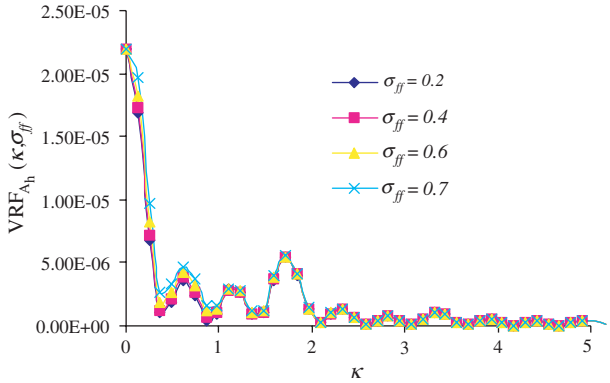

Fig. 18. Variability response function calculated using the FMCS approach for the portal frame in Example 3. Four different values σ_{ff} are considered.

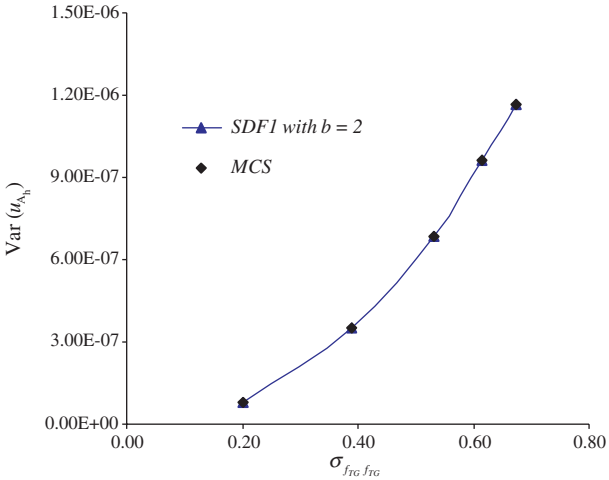

Fig. 19. Example 3: Variance of response displacement u_{A_h} as a function of standard deviation $\sigma_{f_{TG}f_{TG}}$: Comparison of results from the integration of Eq. (24) and from brute-force Monte Carlo simulations (MCS). Plots correspond to a correlation length parameter $b = 2$ of spectral density function SDF1. The corresponding PDF is a truncated Gaussian.

the integration in Eq. (24) and through brute-force Monte Carlo simulations practically coincide, regardless of the value of the standard deviation used for modeling the inverse of the modulus of elasticity. The evolution of the relative error is similar to that shown in Fig. 6. Fig. 20 displays results for $\mathrm{Var}(u_{A_h})$ calculated using the integration in Eq. (24). SDF1 is used to model $S_{ff}(\kappa)$ with standard deviation $\sigma_{ff} = 0.4$. The computed results are plotted as a function of correlation distance parameter b.

Figs. 10, 16 and 20 provide information about the behavior of the variance of the response displacement over the entire range of values of the correlation length parameter of the spectral density function considered. With other available methodologies, the corresponding calculations would require a significant computational effort. The concept of the variability response function not only makes the computational effort trivial, but it also provides an excellent insight on the effect of the shape of $S_{ff}(\kappa)$ through the integral form in Eq. (24).

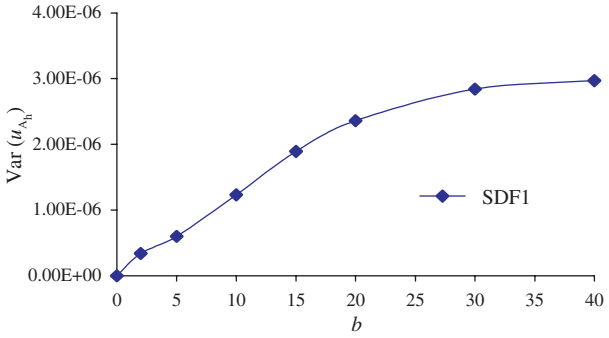

Fig. 20. Example 3: Variance of response displacement u_{A_h} calculated through the integration in Eq. (24) and using SDF1 to model the spectral density function $S_{ff}(\kappa)$. Curve is established for $\sigma_{ff} = 0.4$ and plotted as a function of correlation length parameter b.

5.3.1. Spectral- and probability-distribution-free upper bounds

Spectral- and probability-distribution-free upper bounds for the variance of the response displacement are computed now using Eq. (44). Upper bounds are determined for $\mathrm{Var}(u_{A_h})$ for various values of the standard deviation σ_{ff} of the inverse of the elastic modulus:

$$\mathrm{Var}(u_{A_h}) \leqslant \mathrm{VRF}_{A_h}(\kappa^{\max}, \sigma_{ff} = 0.2) \cdot 0.2^2 = 8.81 \times 10^{-7}; \quad \kappa^{\max} = 0, \tag{68}$$

$$\mathrm{Var}(u_{A_h}) \leqslant \mathrm{VRF}_{A_h}(\kappa^{\max}, \sigma_{ff} = 0.4) \cdot 0.4^2 = 3.53 \times 10^{-6}; \quad \kappa^{\max} = 0, \tag{69}$$

$$\mathrm{Var}(u_{A_h}) \leqslant \mathrm{VRF}_{A_h}(\kappa^{\max}, \sigma_{ff} = 0.6) \cdot 0.6^2 = 7.92 \times 10^{-6}; \quad \kappa^{\max} = 0, \tag{70}$$

$$\mathrm{Var}(u_{A_h}) \leqslant \mathrm{VRF}_{A_h}(\kappa^{\max}, \sigma_{ff} = 0.7) \cdot 0.7^2 = 1.08 \times 10^{-5}; \quad \kappa^{\max} = 0. \tag{71}$$

6. Conclusions

The present paper complemented and extended work done in an earlier study of the authors [3] dealing with the analysis of the response variability of stochastic frame structures. The well-known integral form for the response displacement variance was established in this paper for statically indeterminate structures using a different formulation (applying the concept of non-homogeneous evolutionary fields) that involved an alternative conjecture. The validation of the conjecture was done by comparing the response variance predictions of the integral form with Monte Carlo simulations.

A methodology was provided to determine the variability response function (VRF) (involved in the integral form) numerically through a so-called fast Monte Carlo simulation (FMCS) technique. In addition, closed-form expressions were established for the VRF that indicate a dependence on the standard deviation of the stochastic field modeling the inverse of the elastic modulus, a fact that was validated numerically through the FMCS technique.

Several numerical examples were provided estimating the variance of the response displacement using the integral form in Eq. (24) (in conjunction with a FMCS computation of the VRF) and through brute-force Monte Carlo simulations. The results of the two approaches practically coincided for all cases considered (validating the aforementioned conjecture). Additional numerical examples demonstrated the excellent insight on the effect of the form of the spectral density function of the stochastic field modeling the inverse of the elastic modulus on the response variability. Finally, upper bounds were provided for several cases as a function of the standard deviation of the stochastic field modeling the inverse of the elastic modulus. All computations involving Eq. (24) (determining variance of response and upper bounds) were carried out with minimal computational effort.

Acknowledgements

This work was supported by the National Science Foundation under Grant # CMS-01-15901, with Dr. Peter Chang as Program Director.

References

[1] I. Elishakoff, Y.J. Ren, M. Shinozuka, Some exact solutions for the bending of beams with spatially stochastic stiffness, Int. J. Solids Struct. 32 (16) (1995) 2315–2327.
[2] M. Grigoriu, Applied Non-Gaussian Processes: Examples, Theory, Simulation, Linear Random Vibration, and MATLAB Solutions, Prentice Hall, 1995.
[3] V. Papadopoulos, G. Deodatis, M. Papadrakakis, Flexibility-based upper bounds on the response variability of simple beams, Comput. Methods Appl. Mech. Engrg. 194 (12–16) (2005) 1385–1404.
[4] M.B. Priestley, Non-linear and Non-stationary Time Series Analysis, Academic Press, 1988.
[5] M. Shinozuka, G. Deodatis, Simulation of stochastic processes by spectral representation, Appl. Mech. Rev. 44 (4) (1991) 191–203.